Chapter 3

Maps

(R. Mainieri and P. Cvitanović)

The time parameter in the definition of a dynamical system, sect. 2.1, can be either continuous or discrete. Discrete time dynamical systems arise naturally from flows; one can observe the flow at fixed time intervals (the strobe method), or one can record the coordinates of the flow when a special event happens (the Poincaré section method). This triggering event can be as simple as having one of the coordinates go through a zero, or as complicated as having the flow cut through a curved hypersurface.

3.1 Poincaré sections

Successive trajectory intersections with a *Poincaré section*, a d-dimensional hypersurface or a set of hypersurfaces $\mathcal{P}$ embedded in the $(d+1)$-dimensional phase space $\mathcal{M}$, define the *Poincaré return map* $P(x)$, a d-dimensional map of form

$$x_{n+1} = P(x_n)\,, \qquad x_n, x_{n+1} \in \mathcal{P}\,, \qquad n \in \mathbb{Z}^+ \tag{3.1}$$

(for economy of notation, the *maps* of this chapter will be taken d-dimensional, the associated *flows* $(d+1)$-dimensional). The choice of the section hypersurface $\mathcal{P}$ is altogether arbitrary. With a sufficiently clever choice of a Poincaré section or a set of sections, any orbit of interest intersects a section. Depending on the application, one might need to supplement the return map with the time of *first return function* $\tau(x_n)$ - sometimes referred to as *ceiling function* - which gives the time of flight to the next section for a trajectory starting at x_n, with the accumulated flight time given by

$$t_{n+1} = t_n + \tau(x_n)\,, \qquad t_0 = 0\,, \qquad x_n \in \mathcal{P}\,. \tag{3.2}$$

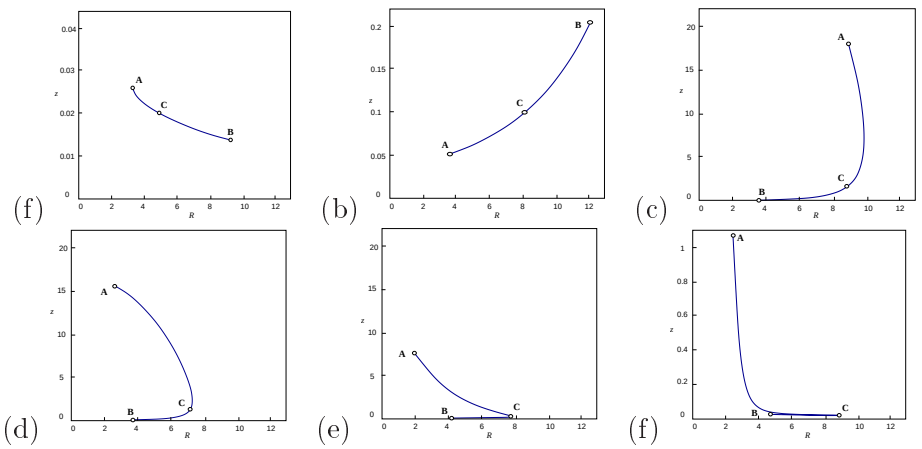

Figure 3.1: A sequence of Poincaré sections of the Rössler flow strange attractor, defined by planes through the z axis, oriented at angles (a) 270^o (b) 135^o, (c) 90^o, (d) 45^o, (e) 0^o, (f) 315^o, in the x-y plane. In order to guide the eye, a continuous line is drawn from a point A on the inner edge of the attractor to the point B on the outer edge (based on a calculation by G. Simon).

Other quantities integrated along the trajectory can be defined in a similar manner, and will need to be evaluated in the process of evaluating dynamical averages.

☞ chapter 8

A few examples may help visualize this.

Example 3.1 Pendulum. *The phase space of a simple pendulum is 2-dimensional: momentum on the vertical axis and position on the horizontal axis. We choose the Poincaré section to be the positive horizontal axis. Now imagine what happens as a point traces a trajectory through this phase space. In the pendulum all orbits are loops, so any trajectory will periodically intersect the line, that is the Poincaré section, at one point. Consider next a pendulum with friction. Now every trajectory is an inward spiral, and the trajectory will intersect the Poincaré section at a series of points that get closer and closer to the origin.*

Pendulum dynamics is so simple that you can sketch it yourself on a piece of paper. Two next two examples offer a better illustration of the utility of visualization of dynamics by means of Poincaré sections.

Example 3.2 Rössler attractor. *Consider fig. 2.3, a typical trajectory of the 3-dimensional Rössler flow (2.11). It wraps around the z axis, so a good choice for a Poincaré section is a plane passing through the z axis. A sequence of such Poincaré sections placed radially at increasing angles with respect to the x axis, fig. 3.1, illustrates the "stretch & fold" action of the Rössler flow. To orient yourself, compare with fig. 2.3, and note the different z axis scales. A line segment $[A, B]$, traversing the width of the attractor, starts out close to the x-y plane, and after the stretching (b) $\to$ (c) $\to$ (d) followed by the folding (d) $\to$ (e) $\to$ (f), the folded segment is returned close to the*

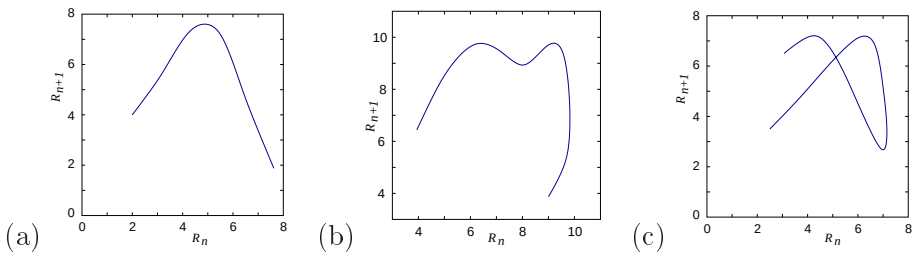

Figure 3.2: Return maps for the $R_n \to R_{n+1}$ radial distance for three distinct Poincaré sections for the Rössler flow, at angles (a) 0^o, (b) 90^o, (c) 45^o around the z-axis, see fig. 3.1. (G. Simon and A. Johansen)

x-y plane strongly compressed. In one Poincaré return the $[A, B]$ interval is stretched, folded and mapped onto itself, so the flow is expanding. *It is also* mixing, *as in one Poincaré return the point C from the interior of the attractor is mapped into the outer edge, while the edge point B lands in the interior.*

Once a particular Poincaré section is picked, we can also exhibit the return map (3.1), as in fig. 3.2. The case (a) is an example of a nice 1-to-1 return map. However, (b) and (c) appear multimodal and non-invertible, artifacts of projections of a 2-dimensional return map $(R_n, z_n) \to (R_{n+1}, z_{n+1})$ onto a 1-dimensional subspace $R_n \to R_{n+1}$.

The dynamics of high-dimensional flows, such as a truncation of the infinite tower of the Kuramoto-Sivashinsky modes (2.17) can be difficult to visualize. The question then is: how to look at such a flow? It is not clear that restricting the dynamics to a Poincaré section necessarily helps - after all, a section reduces a $(d+1)$-dimensional flow to a d-dimensional map, and how much is gained by replacing a continuous flow in 16 dimensionas by a set of points in 15 dimensions? Nevertheless, as we now show, much can be gleaned by examining trajectory's projections onto a subspace spanned by two or three coordinate axes.

Example 3.3 Kuramoto-Sivashinsky attractor. *Consider an N-mode truncation to the infinite tower of the Kuramoto-Sivashinsky coupled Fourier modes (2.17). We fix (arbitrarily) the Poincaré section to be the hyperplane $a_1 = 0$, and integrate (2.17) with the initial conditions $a_1 = 0$, and arbitrary values of the coordinates $a_2, \ldots, a_N$ (where N is the truncation order). When a_1 becomes 0 the next time and the flow crosses the $a_1 = 0$ hyperplane in the same direction as initially, the coordinates $a_2, \ldots, a_N$ are mapped into $(a'_2, \ldots a'_N) = P(a_2, \ldots, a_N)$, where P is the Poincaré mapping (3.1) of the $(N-1)$-dimensional $a_1 = 0$ hyperplane into itself. Fig. 3.3 is an example of a typical result. We have picked - arbitrarily - a subspace such as $a_6(n+1)$ vs. $a_6(n)$ in order to visualize the dynamics. While the topology of the attractor is still obscure, one thing is clear: even though the flow is infinite dimensional, the attractor is finite and thin, barely thicker than a line.*

fast track:
sect. 3.3, p. 55

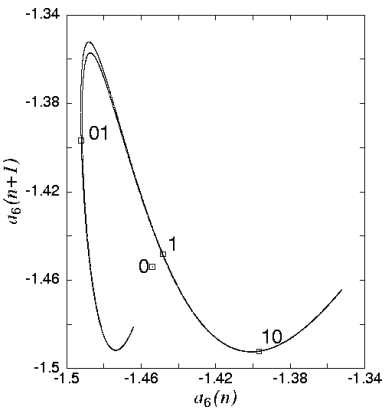

Figure 3.3: The attractor of the Kuramoto-Sivashinsky system (2.17), plotted as the a_6 component of the $a_1 = 0$ Poincaré section return map. Here 10,000 Poincaré section returns of a typical trajectory are plotted. Also indicated are the periodic points 0, 1, 01 and 10. $N = 16$ Fourier modes truncation with $\nu = 0.029910$. (From ref. [2.7].)

The above examples illustrate why a Poincaré section gives a more informative snapshot of the flow than the full flow portrait. For example, while the full flow portrait of the Rössler flow fig. 2.3 gives us no sense of the thickness of the attractor, we see clearly in the Rössler Poincaré sections fig. 3.1 that even though the return map is 2-$d \to$ 2-d, the flow contraction happens to be so strong that for all practical purposes it renders the return map 1-dimensional. Similarly, while no fine structure is discernable in the full flow portraits of Kuramoto-Sivashinsky dynamics fig. 2.5, the Poincaré return map fig. 3.3 reveals the fractal structure in the asymptotic attractor.

3.2 Constructing a Poincaré section

For almost any flow of physical interest a Poincaré section is not available in analytic form. We describe here a numerical method for determining a Poincaré section.

☞ remark 3.1

Consider the system (2.5) of ordinary differential equations in the vector variable $x = (x_1, x_2, \ldots, x_d)$

$$\frac{dx_i}{dt} = v_i(x,t)\,, \tag{3.3}$$

where the flow velocity v is a vector function of the position in phase space x and the time t. In general v cannot be integrated analytically and we will have to resort to numerical integration to determine the trajectories of the system. Our task is to determine the points at which the numerically integrated trajectory traverses a given surface. The surface will be specified implicitly through a function $g(x)$ that is zero whenever a point x is on the Poincaré section. The simplest choice of such section is a plane specified by a point (located at the tip of the vector r_0) and a direction vector a

perpendicular to the plane. A point x is in this plane if it satisfies the condition

3.2 page 61

$$g(x) = (x - r_0) \cdot a = 0\,. \tag{3.4}$$

If we use a tiny step size in our numerical integrator, we can observe the value of g as we integrate; its sign will change as the trajectory crosses the surface. The problem with this method is that we have to use a very small integration time step. In order to actually land on the Poincaré section one might try to interpolate the intersection point from the two trajectory points on either side of the surface. However, there is a better way.

Let t_a be the time just before g changes sign, and t_b the time just after it changes sign. The method for landing exactly on the Poincaré section will be to convert one of the space coordinates into an integration variable for the part of the trajectory between t_a and t_b. Using

$$\frac{dx_k}{dx_1}\frac{dx_1}{dt} = \frac{dx_k}{dx_1}v_1(x,t) = v_k(x,t) \tag{3.5}$$

we can rewrite the equations of motion (3.3) as

$$\frac{dt}{dx_1} = \frac{1}{v_1}\,,\ \cdots\,,\ \frac{dx_d}{dx_1} = \frac{v_d}{v_1}\,. \tag{3.6}$$

Now we use x_1 as the "time" in the integration routine and integrate it from $x_1(t_a)$ to the value of x_1 on the surface, which can be found from the surface intersection condition (3.4). x_1 need not be perpendicular to the Poincaré section; any x_i can be picked as the integration variable, as long as the x_i axis is not parallel to the Poincaré section at the trajectory intersection point. If the section crossing is transverse, v_1 cannot vanish in the short segment bracketed by the integration step preceeding the section, and the point on the Poincaré section.

Of course, once you have determined the Poincaré section point, you use it as the initial point of the next segment of the trajectory, integrated again in the time variable, not in x_1, as globally v_1 vanishes at least twice for each complete Poincaré section return.

3.3 Do it again

Though we have motivated discrete time dynamics by considering sections of a continuous flow, there are many settings in which dynamics is discrete,

and naturally described by repeated applications of the same map

$$f : \mathcal{M} \to \mathcal{M} \,, \tag{3.7}$$

or sequences of consecutive applications of a finite set of maps,

$$\{f_A, f_B, \ldots f_Z\} : \mathcal{M} \to \mathcal{M} \,. \tag{3.8}$$

The discrete "time" is then an integer, the number of applications of a map. As writing out explicitly formulas involving repeated applications of a set of maps can be awkward, we streamline the notation by denoting a map composition by "$\circ$"

$$f_Z(\cdots f_B(f_A(x)))\cdots) = f_Z \circ \cdots f_B \circ f_A(x) \,,$$

and the nth iterate of map f by

$$f^n(x) = f \circ f^{n-1}(x) = f\left(f^{n-1}(x)\right) \,, \qquad f^0(x) = x \,.$$

☞ sect. 2.1

The *trajectory* of x is the set of points

$$\left\{x, f(x), f^2(x), \ldots, f^n(x)\right\} \,,$$

and the *orbit* of x is the subset of all points of $\mathcal{M}$ that can be reached by iterations of f.

The functional form of Poincaré return maps P such as figs. 3.2 and 3.3 can be approximated by tabulating the results of integration of the flow from x to the first Poincaré section return for many $x \in \mathcal{P}$, and constructing a function that interpolates through these points. If we find a good approximation to $P(x)$, we can get rid of numerical integration altogether, by replacing the continuous time trajectory $f^t(x)$ by iteration of the Poincaré return map $P(x)$. Multinomial approximations

$$P_k(x) = a_k + \sum_{j=1}^{d+1} b_{kj} x_j + \sum_{i,j=1}^{d+1} c_{kij} x_i x_j + \ldots \,, \qquad x \in \mathcal{P} \tag{3.9}$$

to Poincaré return maps

$$\begin{pmatrix} x_{1,n+1} \\ x_{2,n+1} \\ \cdots \\ x_{d,n+1} \end{pmatrix} = \begin{pmatrix} P_1(x_n) \\ P_2(x_n) \\ \cdots \\ P_d(x_n) \end{pmatrix} \,, \qquad x_n, x_{n+1} \in \mathcal{P}$$

motivate the study of model mappings of the plane, such as the Hénon map.

Example 3.4 Hénon map. *The map*

$$\begin{aligned} x_{n+1} &= 1 - ax_n^2 + by_n \\ y_{n+1} &= x_n \end{aligned} \tag{3.10}$$

is a nonlinear 2-dimensional map most frequently employed in testing various hunches about chaotic dynamics. The Hénon map is sometimes written as a 2-step recurrence relation

$$x_{n+1} = 1 - ax_n^2 + bx_{n-1}\,. \tag{3.11}$$

An n-step recurrence relation is the discrete time analogue of nth order differential equation, and it can always be replaced by a set of n 1-step recurrence relations.

The Hénon map is the simplest map that captures the "stretch & fold" dynamics of return maps such as the Rössler's, fig. 3.1. It can be obtained by a truncation of a polynomial approximation (3.9) to a Poincaré return map to second order.

A quick sketch of the long-time dynamics of such mapping, such as fig. 3.4, is obtained by picking an arbitrary starting point and iterating (3.10) on a computer. We plot here the dynamics in the (x_n, x_{n+1}) plane, rather than in the (x_n, y_n) plane, because we think of the Hénon map as a model return map $x_n \to x_{n+1}$. As we shall soon see, periodic orbits will be key to understanding the long-time dynamics, so we also plot a typical periodic orbit of such system, in this case an unstable period 7 cycle. Numerical determination of such cycles will be explained in sect. 25.1.

3.4 page 61

Example 3.5 Lozi map. *Another example frequently employed is the* Lozi map*, a linear, "tent map" version of the Hénon map given by*

$$\begin{aligned} x_{n+1} &= 1 - a|x_n| + by_n \\ y_{n+1} &= x_n\,. \end{aligned} \tag{3.12}$$

Though not realistic as an approximation to a smooth flow, the Lozi map is a very helpful tool for developing intuition about the topology of a large class of maps of the "stretch & fold" type.

What we get by iterating such maps is - at least qualitatively - not unlike what we get from Poincaré section of flows, figs. 3.2 and 3.3. For an arbitrary initial point this process might converge to a stable limit cycle, to a strange attractor, to a false attractor (due to the roundoff errors), or diverge. In other words, straight iteration is essentially uncontrollable, and we will need to resort to more thoughtful explorations. As we shall explain in due course below, strategies for systematic exploration rely on stable/unstable manifolds, periodic points, saddle-straddle methods and so on.

3.5 page 62

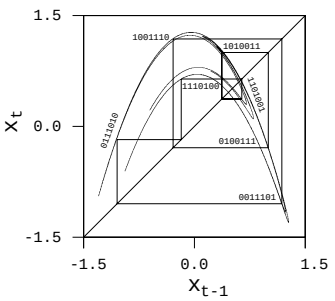

Figure 3.4: The strange attractor and an unstable period 7 cycle of the Hénon map (3.10) with $a = 1.4$, $b = 0.3$. The periodic points in the cycle are connected to guide the eye. (K.T. Hansen [1.3])

Example 3.6 Parabola. *The Hénon map stretches out and folds once a region of the (x, y) plane centered around the origin. Parameter a controls the amount of stretching, while parameter b controls the thickness of the folded image through the "1-step memory" term bx_{n-1} in (3.11). In fig. 3.4 b is rather large, $b = 0.3$, hence the attractor is rather thick, with the transverse fractal structure clearly visible. For vanishingly small b the Hénon map reduces to the 1-dimensional quadratic map*

$$x_{n+1} = 1 - ax_n^2 \,. \tag{3.13}$$

3.6 page 62

By setting $b = 0$ we lose determinism, as on reals the inverse of map (3.13) has two preimages $\{x_{n-1}^+, x_{n-1}^-\}$ for most x_n. Still, this 1-dimensional approximation is very instructive.

As we shall see in sect. 9.4, understanding of 1-dimensional dynamics is indeed the essential prerequisite to unravelling the qualitative dynamics of many higher-dimensional dynamical systems. For this reason many expositions of the theory of dynamical systems commence with a study of 1-dimensional maps. We prefer to stick to flows, as that is where the physics is.

appendix I.4

Commentary

Remark 3.1 Determining a Poincaré section. The idea of changing the integration variable from time to one of the coordinates, although simple, avoids the alternative of having to interpolate the numerical solution to determine the intersection. The trick described in sect. 3.2 was published by Hénon.

Remark 3.2 Hénon, Lozi maps. The Hénon map *per se* is of no particular physical import - its importance lies in the fact that it is a minimal normal form for modeling flows near a saddle-node

bifurcation, and that it is a prototype of the stretching and folding dynamics that leads to deterministic chaos. It is generic in the sense that it can exhibit arbitrarily complicated symbolic dynamics and mixtures of hyperbolic and non–hyperbolic behaviors. Its construction was motivated by the best known early example of "deterministic chaos", the Lorenz equation [2.1]. Y. Pomeau's studies of the Lorenz attractor on an analog computer, and his insights into its stretching and folding dynamics motivated Hénon [3.1] to introduce the Hénon mapping in 1976. Hénon's and Lorenz's original papers can be found in reprint collections refs. [3.2, 3.3]. They are a pleasure to read, and are still the best introduction to the physics motivating such models. Detailed description of the Hénon map dynamics was given by Mira and coworkers [3.4], as well as very many other authors.

The Lozi map [3.6] is particularly convenient in investigating the symbolic dynamics of 2-d mappings. Both the Lorenz and the Lozi system are uniformly smooth maps with singularities. For the Lozi maps the continuity of measure was proven by M. Misiurewicz [3.7], and the existence of the SRB measure was established by L.-S. Young.

☞ sect. 7.1

Résumé

Visualization of strange attractors is greatly facilitated by felicitous choice of Poincaré sections, and reduction of flows to Poincaré section return maps, which motivates study of discrete time dynamical systems generated by iteration of maps.

References

[3.1] M. Hénon, *Comm. Math. Phys.* **50**, 69 (1976).

[3.2] *Universality in Chaos, 2. edition*, P. Cvitanović, ed., (Adam Hilger, Bristol 1989).

[3.3] Bai-Lin Hao, *Chaos* (World Scientific, Singapore, 1984).

[3.4] C. Mira, *Chaotic Dynamics - From one dimensional endomorphism to two dimensional diffeomorphism*, (World Scientific, Singapore, 1987).

[3.5] I. Gumowski and C. Mira, *Recurrances and Discrete Dynamical Systems* (Springer-Verlag, Berlin 1980).

[3.6] R. Lozi, *J. Phys. (Paris) Colloq.* **39**, 9 (1978).

[3.7] M. Misiurewicz, *Publ. Math. IHES* **53**, 17 (1981).

[3.8] B. Eckhardt, *Fractal properties of scattering singularities*, *J. Phys.* **A 20**, 5971 (1987).

[3.9] P. Gaspard and S.A. Rice, *J. Chem. Phys.* **90**, 2225 (1989); **90**, 2242 (1989); **90**, 2255 (1989).

[3.10] P. Cvitanović and B. Eckhardt, "Periodic-orbit quantization of chaotic system", *Phys. Rev. Lett.* **63**, 823 (1989).

[3.11] P. Gaspard and D. Alonso Ramirez, *Phys. Rev.* **A 45**, 8383 (1992).

[3.12] P. Cvitanović and G. Vattay, *Phys. Rev. Lett.* **71**, 4138 (1993).

[3.13] G. Vattay, A. Wirzba and P.E. Rosenqvist, *Phys. Rev. Lett.* **73**, 2304 (1994).

[3.14] D. Fournier, H. Kawakami and C. Mira, *C.R. Acad. Sci. Ser. I,* **298**, 253 (1984); **301**, 223 (1985); **301**, 325 (1985).

[3.15] Ya.G. Sinai, *Usp. Mat. Nauk* **25**, 141 (1970).

[3.16] L.A. Bunimovich, *Funct. Anal. Appl.* **8**, 254 (1974).

[3.17] L.A. Bunimovich, *Comm. Math. Phys.***65**, 295 (1979).

[3.18] L. Bunimovich and Ya.G. Sinai, *Markov Partition for Dispersed Billiard*, *Comm. Math. Phys.* **78**, 247 (1980); **78**, 479 (1980); *Erratum, ibid.* **107**, 357 (1986).

[3.19] M. Benedicks and L.-S. Young, *Ergodic Theory & Dynamical Systems* **12**, 13–37 (1992).

[3.20] H.J. Korsch and H.-J. Jodl, *Chaos. A Program Collection for the PC*, (Springer, New York 1994)